ORIGINAL PAPER

Effect of Tangential Loading History on Static Friction Force of Elastic Slider with Split Contact Surface: Model Calculation

Satoru Maegawa[1] · Fumihiro Itoigawa[2] · Takashi Nakamura[2] · Hiroshige Matsuoka[1] · Shigehisa Fukui[1]

Abstract This study provides a novel insight into the study of static friction force. From numerical simulations with a simplified sliding model in which the friction force between an elastic slider with a split contact interface and a rigid base block with a smooth surface was analyzed, it was found that the existence of the stop–restart motion works to increase static friction force, while the stop–inversion motion reduces static friction force. Thus, the numerical simulations in this study demonstrated that the magnitude of static friction force varies with different types of tangential loading sequences. Furthermore, it was found from an analytical discussion that the magnitude of this tangential loading history effect is characterized by the dispersion level of the threshold lengths for the onset of slip motion at each contact point and also by the ratio of kinetic friction coefficient to static friction coefficient at the contact interface. Through the previously mentioned analytical approaches, this study emphasizes that the sequence of tangential loading is an important factor for characterizing the magnitude of static friction force.

Keywords Static friction · Tangential loading history · Elastomer · Split contact surface

✉ Satoru Maegawa
maegawa@damp.tottori-u.ac.jp

[1] Department of Mechanical and Aerospace Engineering, Tottori University, 4-101 Minami, Koyama, Tottori 680-8553, Japan

[2] Department of Mechanical Engineering, Nagoya Institute of Technology, Gokiso-cho Showa-ku, Nagoya, Aichi 466-8555, Japan

List of symbols

A	Fitting parameter used in Eqs. (9)–(11)
c^i	Viscosity at ith contact point
δk^i	Small statistical deviations of k^i distribution
δf_z^i	Small statistical deviations of f_z^i distribution
f_k^i	Local kinetic friction force at ith contact point
f_s^i	Local static friction force at ith contact point
$\bar{f}_k$	Averaged values of f_k^i of the contact points under slip states
$\bar{f}_s$	Averaged values of f_s^i of the contact points under stick states
F_{smax}	(Maximum) static friction force
F_{smax}^{1st}	(Maximum) static friction force at 1st loading period
F_{smax}^{2nd}	(Maximum) static friction force at 2nd loading period
F_{smax}^{3rd}	(Maximum) static friction force at 3rd loading period
f_{smax}^i	Maximum static friction force at ith contact point
f_x^i	Local tangential force at ith contact point
F_x	Total tangential force
f_z^i	Local normal load at ith contact point
F_z	Total normal load
k^i	Tangential stiffness at ith contact point
K	Total tangential stiffness
l_{ini_c}	Center value of l_{ini} distribution
l_{SI_c}	Center value of l_{SI} distribution
l_{SR_c}	Center value of l_{SR} distribution
l^i	Threshold length for the onset of slip motion
$l_{effective}^i$	Effective threshold length
l_{ini}^i	Threshold length at 1st loading period

| $l^i_{residual}$	The stored strain length at ith contact point in the stopping period
l^i_{SI}	Threshold length at SI motion
l^i_{SR}	Threshold length at SR motion
m^i	Mass at ith contact point
N	Number of contact points
N_{slip}	Number of contact points under slip state
N_{stick}	Number of contact points under stick state
$P(l)$	Probability distribution function of l
$P_{ini}(l_{effective})$	Probability distribution function of $l_{effective}$ at 1st loading period
$P_{SI}(l_{effective})$	Probability distribution function of $l_{effective}$ at SI motion
$P_{SR}(l_{effective})$	Probability distribution function of $l_{effective}$ at SR motion
U	Macroscopic displacement
u^i	Displacement at ith contact point
V	Driving speed
ΔF_{x_ini}	Difference between static and kinetic friction forces at initial motion defined in Fig. 6
ΔF_{x_SI}	Difference between static and kinetic friction forces at SI motion defined in Fig. 6
ΔF_{x_SR}	Difference between static and kinetic friction forces at SR motion defined in Fig. 6
λ_K	Variation parameter of k^i distribution
λ_{Fz}	Variation parameter of f^i_z distribution
μ_k	Kinetic friction coefficient
μ_s	Static friction coefficient
σ_{ini}	Standard deviation of l_{ini} distribution
σ_{SI}	Standard deviation of l_{SI} distribution
σ_{SR}	Standard deviation of l_{SR} distribution
χ_{SI}	Increasing ratio of static friction force at SI motion
χ_{SR}	Increasing ratio of static friction force at SR motion

1 Introduction

Static friction force is an important factor for determining the capabilities of sliding systems. A large static friction force is effective to prevent unnecessary slippage. On the other hand, in some cases, a low static friction force is required to achieve a smooth start motion without unstable slippage because large static friction sometimes causes an unstable sliding motion, such as stick–slip vibration [1, 2]. For the above reasons, designing static friction force has been an important issue in the study of friction, especially in mechanical engineering.

One of the methods for designing static friction force is based on the use of surface textures, which includes artificial surface structures ranging from μm to mm scales. For example, as experimentally and theoretically demonstrated, the use of a split contact interface is an effective method to reduce the level of static friction force [3–9]. When a split contact interface slides on a rigid smooth plane, the transition from static to kinetic friction at each contact region occurs independently at different times because the local stiffness and normal load at each contact region are not perfectly equal to each other. Therefore, the local static friction force that appears in the local scale is canceled at the macroscopic scale. When a time change in macroscopic friction force is focused on, a smooth start motion is often observed, even if a local stick–slip motion occurs at each contact point.

In the previous report by Maegawa et al. [10], it was pointed out that the existence of the stop–restart (SR) motion works to increase macroscopic static friction force, based on numerical and experimental results focusing on the sliding friction of a rubber slider with a split contact interface. In this study, the effect of SR motion on static friction force is reported again with some additional discussions. In addition, as a new insight, the effect of stop–inversion (SI) motion on static friction force is discussed. From numerical simulations, it was found that SI motion reduces static friction force, in contrast to the case for SR motion. Furthermore, the mechanism of this tangential loading history dependence of static friction force is also discussed.

2 Analytical Model

Figure 1 shows a schematic illustration of the analytical model used in this study, which was already developed in the previous study by Maegawa et al. [10]. The model is based on a simplified analytical model developed by Kligerman and Varenberg [7], which suggested treating dynamic stick–slip phenomena in terms of massless quasi-static approach based on the difference between static and kinetic friction. In order to facilitate discussion, the details of this model are described again. This model represents the sliding friction between an elastic split surface with multiple contact points and a rigid smooth plane that moves in the x direction with a driving speed of V. The contact interface is divided into N contact points, and the ith contact point is connected to the bulk region via a spring with a stiffness of k^i. It should be noted that to simplify the analysis, the mass of the contact point, m^i, and the viscosity at the connection, c^i, were set to zero values: $m^i = 0$ and $c^i = 0$. In addition, the interaction between neighboring
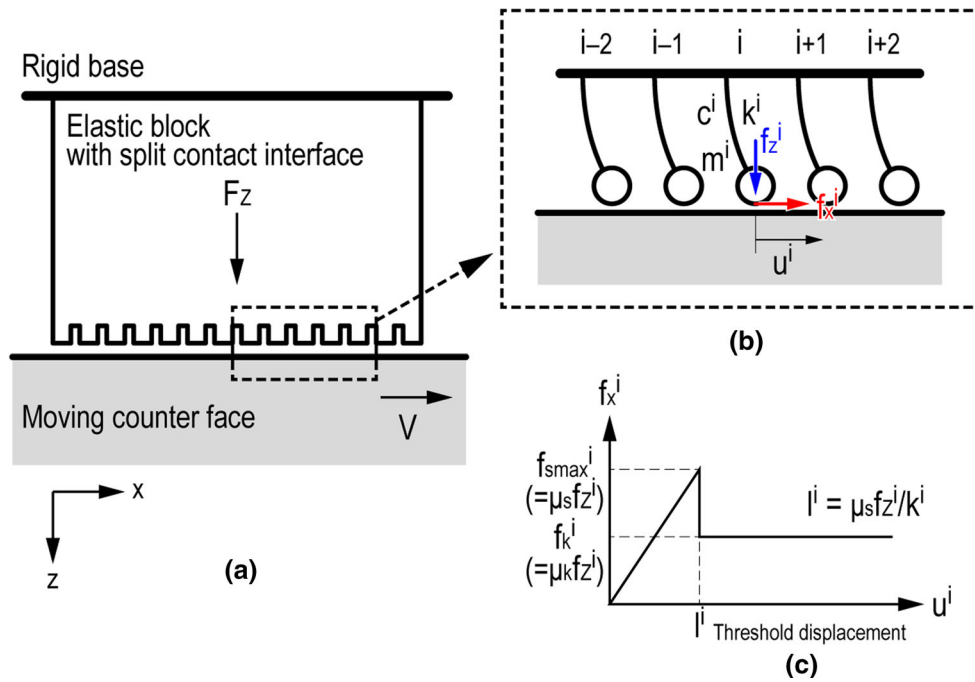
Fig. 1 Schematic diagram of the analytical model

contacts points was not considered; all of the contact points were connected to the bulk region independently. Therefore, dynamic behaviors, such as crack propagation [11–13], were not considered in this study. At each contact point, a local normal load, f_z^i, was applied on the contact interface, and a local tangential force, f_x^i, also acts along the tangential direction.

As discussed by Farkas et al. [14], the coherence of the contact interface, which is the magnitude of the dispersion in the distribution of threshold lengths for the onset of slip at each contact point, is an important factor for characterizing the level of macroscopic static friction force in a split (or rough) contact interface. Similarly, Kligerman and Varenberg [7] numerically analyzed the effect of the distributions on the local stiffness of k^i and the effects of the local normal load, f_z^i, on macroscopic static friction force.

In this study, based on the description by Kligerman and Varenberg, the stiffness of the spring, k^i, and the local normal load, f_z^i, are statistically scattered as:

$$k^i = K/N + \delta k^i$$
$$f_z^i = F_z/N + \delta f_z^i, \quad (1)$$

where K and F_z are the total tangential stiffness and the normal load, respectively. Here, the dispersions of stiffness and normal load distributions are characterized by δk^i and δf_z^i, which represent small statistical deviations (positive or negative) of those parameters from their average values. The random values of δk^i and δf_z^i are chosen using a random number generator with a Gaussian distribution. Here,

the mean values of the distributions of k^i and f_z^i correspond to K/N and F_z/N, respectively. In addition, the standard deviations of these distributions are formulated as $\lambda_K K/N$ and $\lambda_{Fz} F_z/N$, respectively. Therefore, the level of their variation is characterized by the values of λ_K and λ_{Fz}.

The motion of each contact point is governed by the force balance between the spring force and friction force; thus, $k^i u^i = f_x^i$. Here, u^i, which is denoted in Fig. 1b, is the displacement that originates from the position under the natural length of the spring of the ith contact point, and f_x^i is the local friction force that acts on the contact between the ith contact point and the counter face. The relationship between f_x^i and u^i is illustrated in Fig. 1c, where l^i is the threshold displacement for the onset of the transition from static to kinetic friction at each contact point. Considering that the maximum static friction force is described as $f_{smax}^i = \mu_s f_z^i$, where μ_s is the static friction coefficient, l^i can be formulated as $\mu_s f_z^i / k^i$. Thus, f_x^i is described by:

$$f_x^i = \begin{cases} f_s^i = k^i u^i & \text{when in the stick state, i.e., } u^i < l^i \\ f_k^i & \text{when in the slip state, i.e., } u^i \geq l^i \end{cases}. \quad (2)$$

Here, $l^i = \mu_s f_z^i / k^i$. On the other hand, in the slip state, the local kinetic friction force f_k^i is described as $f_k^i = \mu_k f_z^i$, where μ_k is the kinetic friction coefficient. This study does not consider the velocity dependence of the kinetic friction coefficient and assumes that $\mu_s > \mu_k$. Here, the total tangential force, F_x, was determined by the sum of the local friction forces; thus,

$$F_x = \sum f_x^i = \bar{f}_s N_{\text{stick}} + \bar{f}_k N_{\text{slip}}, \quad (3)$$

where $\bar{f}_s$ and $\bar{f}_k$ are the averaged values of f_s^i and f_k^i of the contact points under stick and slip states, respectively. In addition, N_{stick} and N_{slip} are the number of masses under stick or slip states, respectively. Here, $N_{stick} + N_{slip} = N$. It should be noted that in this study, for a simple description, the term "static friction force" is used in referring to "maximum static friction force."

The four types of tangential loading sequences focused on in this study are illustrated in Fig. 2, in which time changes in the driving velocity V of the moving counter face are shown. In all cases, the loading sequence includes three loading periods (LPs), 1st LP, 2nd LP, and 3rd LP, and two stopping periods (SPs). During the SP, $V = 0$. For example, in the SR–SR motion (Fig. 2a), during all LPs, V has a positive value. In contrast, in the SR–SI motion (Fig. 2b), in the first and second LPs, V is positive; while in the third LP, V is negative. In addition, in Fig. 2, two different types of basic motions (SI motion and SR motion) are included in the four loading sequences and are represented using large color arrows. Here, "SR motion" refers to the stop–restart motion, in which the sign of V does not
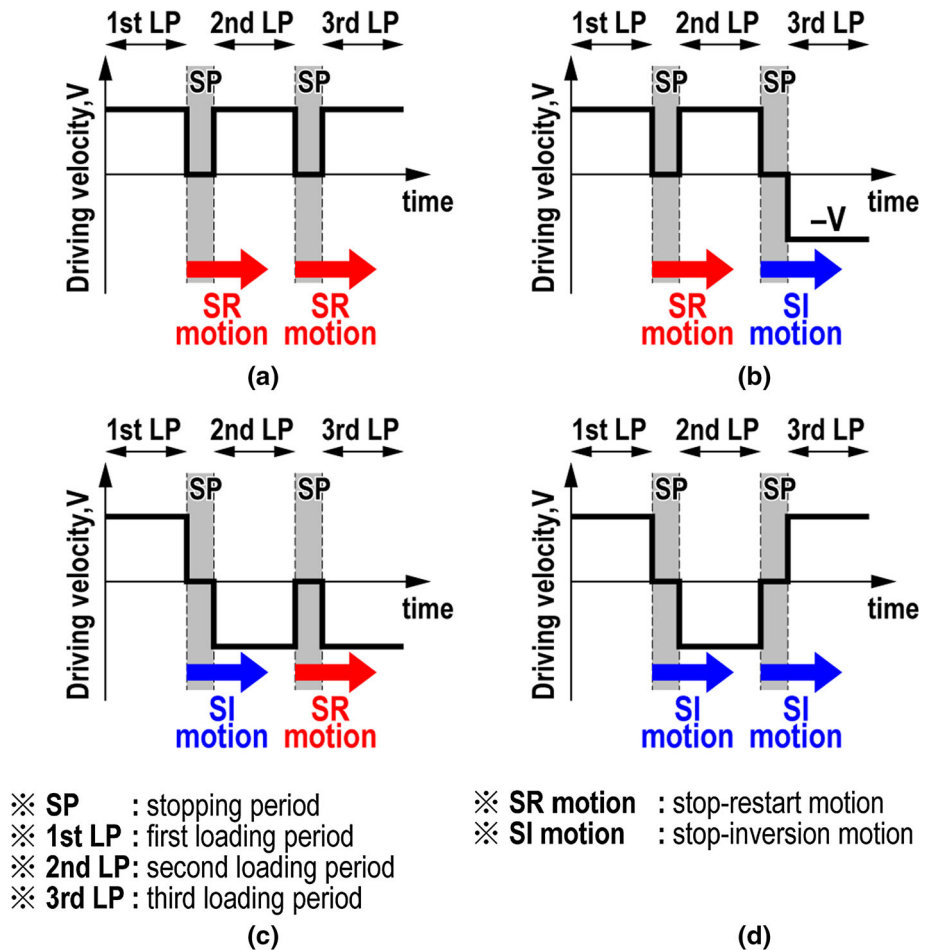
Fig. 3 Time changes in V (*top*), F_X (*middle*), and N_{stick}/N (*bottom*) ▶ under the SR–SR, SR–SI, SI–SR, and SI–SI motions: $F_z = 10$ N, $K = 1$ N/μm, $\mu_s = 1.0$, $\mu_k = 0.5$, $N = 1000$, $\lambda_K = 0.1$,   and $\lambda_{Fz} = 0.1$
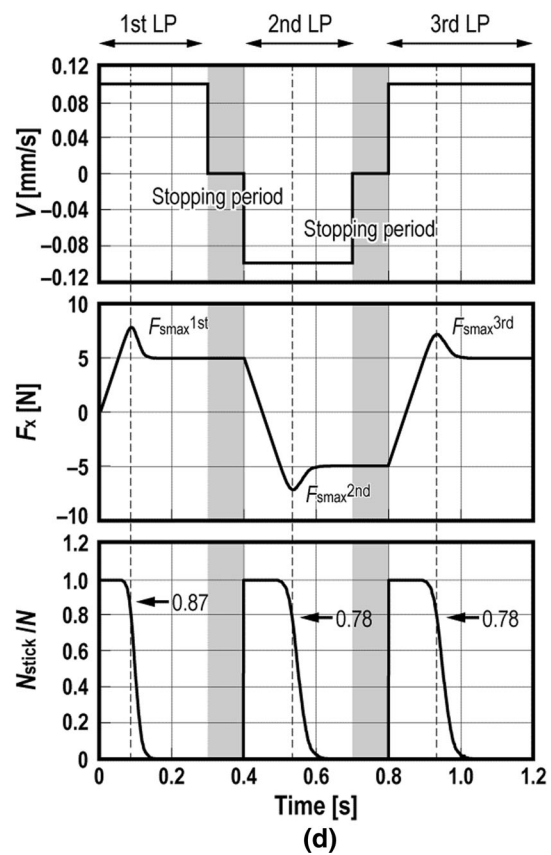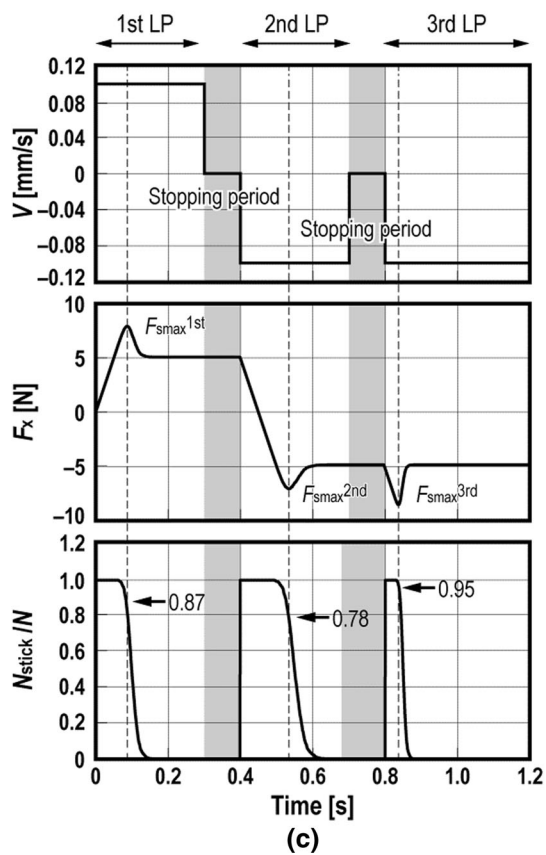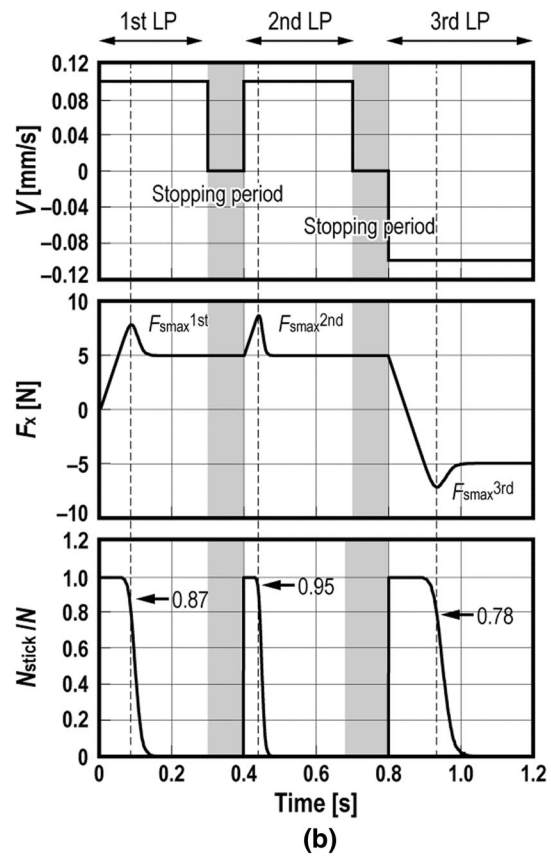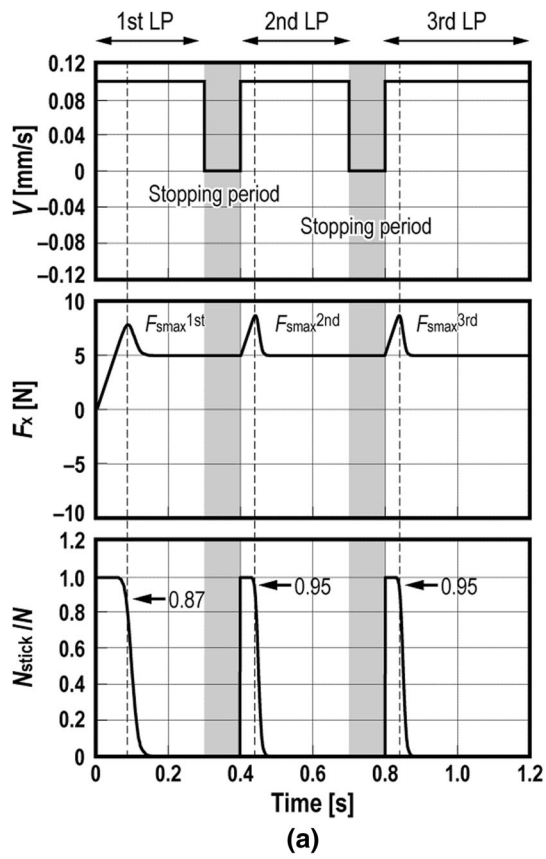
change before or after the SP. In contrast, "SI motion" refers to the stop-inversion motion, in which the sign of V changes before and after the SP. Therefore, for example, the SR–SR motion includes two SR motions, and the SI–SI motion includes two SI motions, as illustrated in Fig. 2.

3 Results

Figure 3 shows calculation results under four types of loading sequences: (a) SR–SR, (b) SR–SI, (c) SI–SR, and (d) SI–SI motions. Based on the above descriptions, time changes in driving velocity (V), total tangential force (F_x) calculated by Eq. (3), and the ratio of the mass number under stick condition N_{stick} on the total mass number (N) are presented. The gray bands between the first and second LPs and between the second and third LPs depict

Fig. 2 Schematic illustration of the four types of tangential loading sequences considered in this study

※ **SP**   : stopping period
※ **1st LP** : first loading period
※ **2nd LP**: second loading period
※ **3rd LP** : third loading period

※ **SR motion** : stop-restart motion
※ **SI motion** : stop-inversion motion

(a)

(b)

(c)

(d)

the SP, where $V = 0$ mm/s. The top graphs in Fig. 3 correspond to the illustration in Fig. 2. The calculation conditions are as follows: $F_z = 10$ N, $K = 1$ N/μm, $V = 0.1$ mm/s, $\mu_s = 1.0$, $\mu_k = 0.5$, $N = 1000$, $\lambda_K = 0.1$, and $\lambda_{Fz} = 0.1$.

From the middle graph in Fig. 3a, it was found that in the SR–SR motion, the first static friction force F_{smax}^{1st}, which is defined as the maximum value of F_x during the first LP, is lower than F_{smax}^{2nd} and F_{smax}^{3rd}; thus, $F_{smax}^{1st} < F_{smax}^{2nd} = F_{smax}^{3rd}$. Similarly, in the other three loading sequences, depicted in Fig. 3b–d, F_{smax}^{2nd} and F_{smax}^{3rd} do not equal F_{smax}^{1st}. The changes in F_{smax} due to the change in the tangential loading sequence are summarized in Fig. 4. It should be noted that the vertical axis in Fig. 4 represents the absolute values of static friction force, i.e., $|F_{smax}|$. It is clear that after the SR motion, $|F_{smax}|$ increases from its value at the first LP; while after the SI motion, it decreases from its value at the first LP. Therefore, it was determined that F_{smax} depends on the type of tangential loading sequence. The mechanism of the effect of the tangential loading history on static friction force will be discussed in the following section.

The bottom graphs in Fig. 3 show the changes in N_{stick}/N. At the initial condition when time is 0 s, N_{stick}/N is unity because all of the contact points are under the stick state.
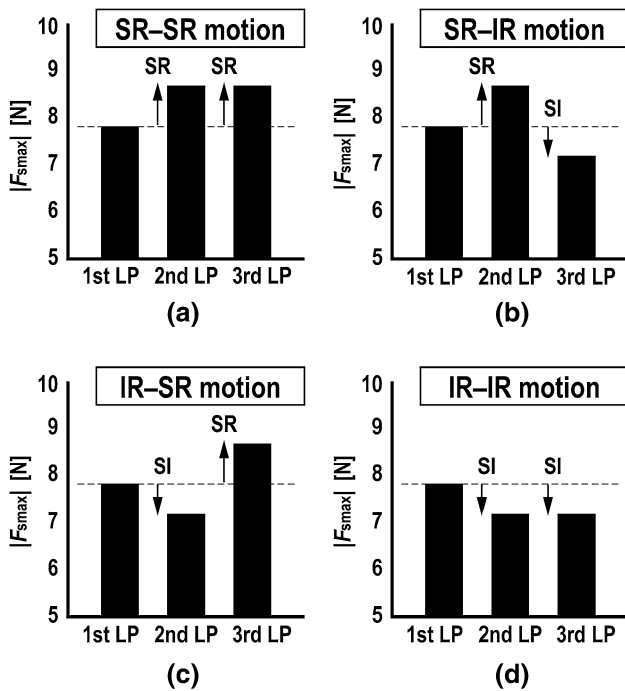
After the onset of the driving motion, N_{stick}/N decreases with time, and then, reaches a zero value when global slip is established. The values of N_{stick}/N when $F_x = F_{smax}^{1st}$, $F_x = F_{smax}^{2nd}$, and $F_x = F_{smax}^{3rd}$ are also depicted in Fig. 3. Comparing with each of the loading sequences, it was found that during the SR motion, N_{stick}/N at $F_x = F_{smax}^{2nd}$, or $F_x = F_{smax}^{3rd}$ increases from the value at $F_x = F_{smax}^{1st}$; while during the SI motion, they decrease from the values at $F_x = F_{smax}^{1st}$. For example, in the SR–SI motion (Fig. 3b), during the SR motion, N_{stick}/N at $F_x = F_{smax}^{2nd}$ is 0.95, but during the SI motion, N_{stick}/N at $F_x = F_{smax}^{2nd}$ is 0.78. As formulated in Eq. (3), the value of the macroscopic tangential force, F_x, is characterized by N_{stick} and N_{slip}, where $N_{slip} = N - N_{stick}$. Here, N_{stick} is described using a probability distribution function of the threshold length, l, i.e., $P(l)$,

$$N_{stick} = N \int_U^\infty P(l) \mathrm{d}l, \tag{4}$$

where U is the macroscopic sliding distance (displacement), and $\int_0^\infty P(l)\mathrm{d}l = 1$. From Eq. (4), it is obvious that the magnitude of the dispersion of the threshold length distribution characterizes the value of N_{stick} at the macroscopic sliding distance U, and it determines the value of F_x. Therefore, considering that the magnitude of static friction force is characterized by the value of N_{stick}/N, as shown in Fig. 3, it was found that the coherence of the threshold length, l, is an important factor for determining the macroscopic static friction force. The role of the coherence on friction has been already pointed out in the reference in [14], based on the theoretical analysis. Thus, the static friction force of the slider with a relatively high coherence of the threshold length is larger than that with a low coherence slider.

4 Discussion

We considered the mechanism of the effect of tangential loading history on static friction force. From the above discussion, it was found that the threshold length distribution, i.e., $P(l)$, affects the magnitude of the static friction force. Therefore, in this section, we focused on the changes in $P(l)$ during the tangential loading sequences. Here, we again define the threshold length for the onset of the transition from static to kinetic friction. When the spring k^i is perfectly relaxed before applying tangential loading, l^i can be described by $\mu_s f_z^i / k^i$, as denoted in Fig. 1. However, in many cases, a certain strain is stored in the contact interface before tangential loading, i.e., $l_{residual}^i \neq 0$ and $l^i \neq \mu_s f_z^i / k^i$. Therefore, the effective

Fig. 4 Changes in static friction force during three loading periods in the SR–SR, SR–SI, SI–SR, and SI–SI motions: $F_z = 10$ N, $K = 1$ N/μm, $\mu_s = 1.0$, $\mu_k = 0.5$, $N = 1000$, $\lambda_K = 0.1$, and $\lambda_{Fz} = 0.1$

threshold length, $l_{\text{effective}}^i$, which varies with time during tangential loading sequence, should be defined as

$$l_{\text{effective}}^i = \mu_s f_z^i / k^i - l_{\text{residual}}^i. \tag{5}$$

Here, it is clear that the value of l_{residual}^i at the jth loading period (LP) is determined by the kinetic friction force at the $j - 1$th LP because during the SP, the strain of the ith spring for the kinetic friction that is applied during the $j - 1$th LP is stored for the jth LP. Thus, l_{residual}^i at the second LP is determined by the value of f_k^i at the first LP, and l_{residual}^i at the third LP is determined by the value of f_k^i at the second LP. On the other hand, l_{residual}^i at the first LP is zero value because no residual strain is stored before the start of the first tangential loading. Consider that after the SR motion the sign of f_k^i does not change; while after the SI motion, f_k^i after the SP is the opposite sign as before the SP,

$$|l_{\text{effective}}^i| = \begin{cases} \dfrac{\mu_s f_z^i}{k^i} & \text{at 1st LP} \\[2mm] \dfrac{\mu_s f_z^i}{k^i} - \dfrac{\mu_k f_z^i}{k^i} & \text{at SR motion} \\[2mm] \dfrac{\mu_s f_z^i}{k^i} + \dfrac{\mu_k f_z^i}{k^i} & \text{at SI motion} \end{cases} \tag{6}$$
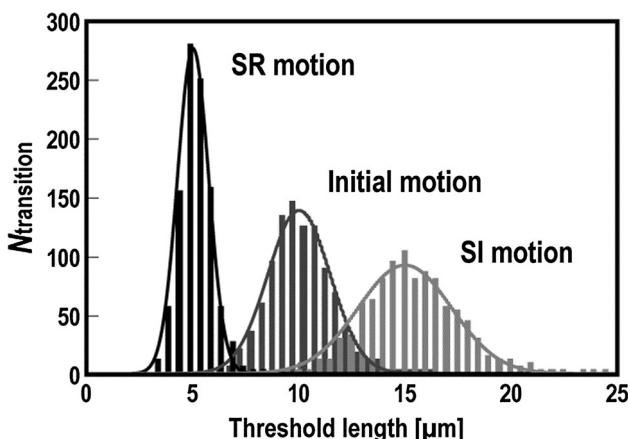
Using the following relationship:

$$l_{\text{ini}}^i = \frac{\mu_s f_z^i}{k^i}, \tag{7}$$

Equation (6) can be written as

$$|l_{\text{effective}}^i| = \begin{cases} l_{\text{ini}}^i & \text{at 1st LP} \\[2mm] l_{\text{SR}}^i = l_{\text{ini}}^i \left(1 - \dfrac{\mu_k}{\mu_s}\right) & \text{at SR motion} \\[2mm] l_{\text{SI}}^i = l_{\text{ini}}^i \left(1 + \dfrac{\mu_k}{\mu_s}\right) & \text{at SI motion} \end{cases} \tag{8}$$

From Eq. (8), the changes in the effective threshold length, $l_{\text{effective}}^i$, during the tangential loading sequence

Fig. 5 Histograms for threshold length. *Black bars* SR motion, *dark gray bars* initial motion, and *gray bars* SI motion

were quantified. Thus, the changes in the distribution of $l_{\text{effective}}^i$ during the changes in tangential loading sequence are characterized by the factor μ_k/μ_s.

Figure 5 shows histograms of the distributions of $l_{\text{effective}}^i$, which were calculated using Eq. (6). The black, dark gray, and gray bars represent $l_{\text{effective}}^i$ distributions for the SR, initial, and SI motions, respectively. It is obvious that the dispersion of $l_{\text{effective}}^i$ for the SR motion is smaller than that at the initial motion. In contrast, the dispersion for the SI motion is larger than that at the initial motion. In this study, it is assumed that a probability distribution function at the initial motion $P_{\text{ini}}(l_{\text{effective}})$ can be described by using the Gaussian function. Therefore, $P_{\text{ini}}(l_{\text{effective}})$ is determined by a fitting process as

$$\begin{aligned} P_{\text{ini}}(l_{\text{effective}}) &= \frac{A}{\sqrt{2\pi\sigma_{\text{effective}}^2}} \exp\left(-\frac{(l_{\text{effective}} - l_{\text{effective\_c}})^2}{2\sigma_{\text{effective}}^2}\right) \\ &= \frac{A}{\sqrt{2\pi\sigma_{\text{ini}}^2}} \exp\left(-\frac{(l_{\text{ini}} - l_{\text{ini\_c}})^2}{2\sigma_{\text{ini}}^2}\right), \end{aligned} \tag{9}$$

where A and σ_{ini} are fitting parameters, which were determined to be $A = 512$, and $\sigma_{\text{initial}} = 1.45$ μm. In addition, it is assumed that the center value of the distribution $l_{\text{ini\_c}}$ is $l_{\text{ini\_c}} = \mu_k Fz/K$. Here, from Eq. (8), the following relationships are obtained: $l_{\text{SR}}^i = l_{\text{ini}}^i (1 - \mu_k/\mu_s)$, $l_{\text{SR\_c}} = l_{\text{ini\_c}}(1 - \mu_k/\mu_s)$, $l_{\text{SI}}^i = l_{\text{ini}}^i (1 + \mu_k/\mu_s)$, and $l_{\text{SI\_c}} = l_{\text{ini\_c}} (1 + \mu_k/\mu_s)$. Therefore, the probability distribution functions at the SR and SI motions, i.e., $P_{\text{SR}}(l_{\text{effective}})$ and $P_{\text{SI}}(l_{\text{effective}})$, are described as

$$P_{\text{SR}}(l_{\text{effective}}) = \frac{A}{\sqrt{2\pi\sigma_{\text{SR}}^2}} \exp\left(-\frac{(l_{\text{SR}} - l_{\text{SR\_c}})^2}{2\sigma_{\text{SR}}^2}\right) \tag{10}$$

and

$$P_{\text{SI}}(l_{\text{effective}}) = \frac{A}{\sqrt{2\pi\sigma_{\text{SI}}^2}} \exp\left(-\frac{(l_{\text{SI}} - l_{\text{SI\_c}})^2}{2\sigma_{\text{SI}}^2}\right), \tag{11}$$

where $\sigma_{\text{SR}} = \sigma_{\text{ini}}(1 - \mu_k/\mu_s)$ and $\sigma_{\text{SI}} = \sigma_{\text{ini}}(1 + \mu_k/\mu_s)$. The black and gray curves for the SR and SI motions in Fig. 7 are based on Eqs. (10) and (11), respectively. Considering that the magnitude of the static friction force is determined by the coherence of the threshold length distribution, which is characterized by σ_{ini}, $\sigma_{\text{SR}}(=\sigma_{\text{ini}}(1 - \mu_k/\mu_s))$, and $\sigma_{\text{SR}}(=\sigma_{\text{ini}}(1 + \mu_k/\mu_s))$, it was determined that the factor μ_k/μ_s is an important factor for determining the magnitude of the changes in static friction force due to the existence of SR or SI motions.

In order to quantify the magnitude of the tangential loading history dependence of static friction force, the following parameters are defined:

Fig. 6 Definitions of ΔF_{x_ini}, ΔF_{x_SR}, and ΔF_{x_SI} used in Eqs. (12) and (13)
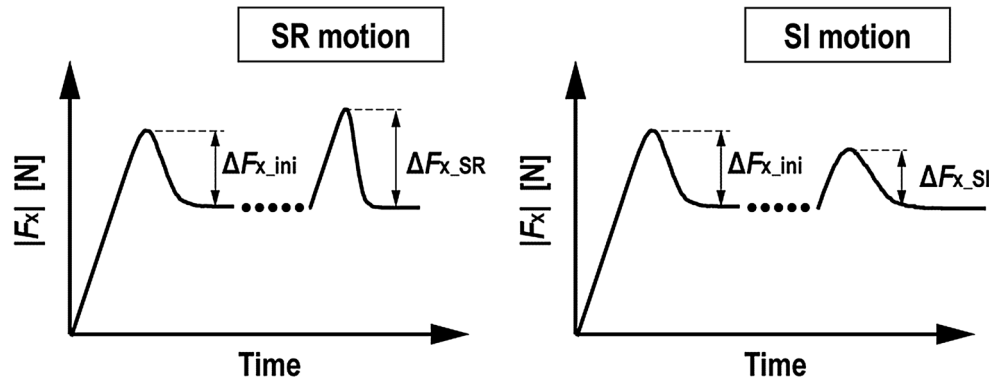
$$\chi_{SR} = \frac{\Delta F_{x\_SR}}{\Delta F_{x\_ini}} \qquad (12)$$

and

$$\chi_{SI} = \frac{\Delta F_{x\_SI}}{\Delta F_{x\_ini}}, \qquad (13)$$

where the meanings of ΔF_{x_ini}, ΔF_{x_SR}, and ΔF_{x_SI} are illustrated in Fig. 6. Here, it should be noted that the vertical axis of Fig. 6 represents the absolute value of F_x. When χ_{SR} has a large value, the static friction force largely increases because of the SR motion. On the other hand, a small χ_{SI} means that a large decrement of static friction force due to the SI motion occurs.

Figure 7 shows the relationship between χ_{SR} or χ_{SI} and the factor μ_k/μ_s under different λ_K and λ_{Fz}. From the figure, it is seen that χ_{SR} (or χ_{SI}) monotonically increases (or decreases) as μ_k/μ_s increases. This indicates that when μ_k has a relatively large value, a large effect of the tangential loading history on static friction force is observed. In contrast, in the case for $\mu_k = 0$, the tangential loading history dependence of static friction force is not observed. It is easily understood from Eq. (6); when $\mu_k = 0$, the value of $l_{effective}^i$ does not change during the tangential

loading sequence. Thus, the value of static friction force does not depend on the type of tangential loading sequence. In addition, from Fig. 7, it was found that when the dispersion of the local tangential stiffness and local normal load has large values, there is a large tangential loading history dependence.

From Fig. 7, it was also found that a macroscopic static friction force depends not only on local static friction force but also on local kinetic friction force. As described in Eq. (3), the change in total tangential force, F_x, includes local static friction force, f_s, and also the local kinetic friction force, f_k. Therefore, the optimization of kinetic friction force is one of the options for designing the macroscopic static friction. Thus, it was found that the development process of micro-slip that occurs prior to global slip, which characterizes the changes in N_{stick} and N_{slip} during tangential loading, is an important factor for determining the static friction force. In addition, this study newly presents the finding that static friction force can be adjusted by controlling surface topography focusing on the coherence of the distribution of threshold length.

The analytical model used in this study is based on the Amonton–Coulomb friction laws; thus, friction coefficients do not depend on normal load, and kinetic friction force is

Fig. 7 Relationships between a χ_{SR} and μ_k/μ_s and b χ_{SI} and μ_k/μ_s under different λ_K and λ_{Fz}; $F_z = 10$ N, $K = 1$ N/μm, $\mu_s = 1.0$, $\mu_k = 0.5$, and $N = 1000$
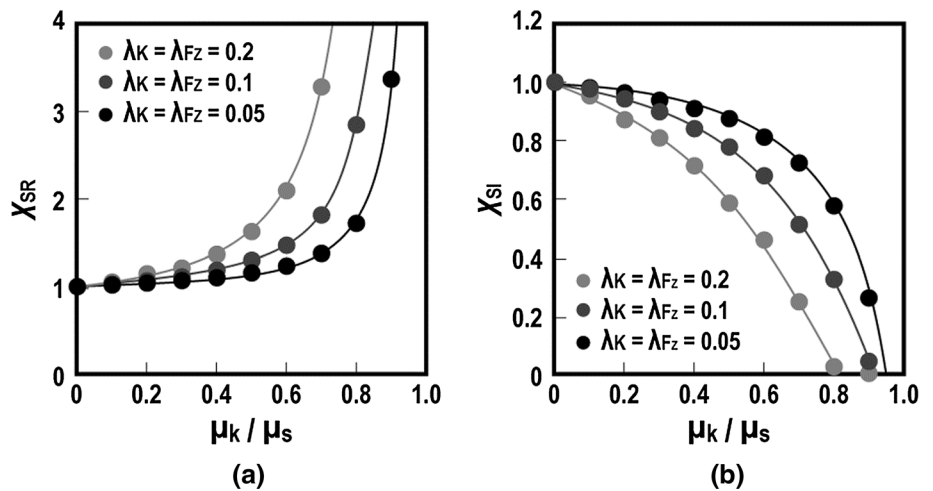
constant for the change in sliding speed. However, in the case of friction in polymers, the Amonton–Coulomb friction laws are not even broadly applicable. The friction coefficients depend on normal load, sliding speed, and other conditions [15, 16]. Therefore, the magnitude of the effect of the tangential loading history on static friction force will depend on a number of conditions, including sliding speed, normal load, temperature, and surface roughness.

Similar to the case of the effect of tangential loading history on static friction force, the effect of normal loading history on static friction force has been discussed [17–19]. The essence of the normal and tangential loading history dependence is the same; static friction force is characterized by the magnitude of the initial strain distribution, which affects the development process of micro-slip and also characterizes the macroscopic static friction force. Therefore, the control of the micro-slip propagation, focusing on the tangential or normal loading sequence, can design macroscopic static friction force. Finally, it is noted that, as presented in the previous research [20], the tangential loading history dependence of static friction force can be observed in another sliding system, in which a continuous sliding interface is considered instead of the split contact interface.

5 Conclusions

Through numerical analysis, tangential loading history dependence of static friction force was discussed, focusing on the sliding friction between an elastic slider with a split contact interface and a rigid flat surface. Consequently, it was found that the existence of the stop–restart (SR) motion works to increase static friction force compared to the static friction force under nonresidual surface strain conditions. In contrast, the SI motion reduces static friction force compared to that under no surface strain conditions. In addition, it was found that the coherence of the distribution of threshold length for the onset of transition from static to kinetic friction at each contact point characterizes the magnitude of the effect of tangential loading history on static friction force. Furthermore, the ratio of kinetic friction coefficient on static friction coefficient also characterizes the tangential loading history effect. Therefore, when kinetic friction coefficient has a relatively large value, a large tangential loading history effect is observed. Because the SR and SI motions are basic behaviors in many sliding systems, the effect of the tangential loading history on static friction force is an important consideration

for improvements in the capabilities of systems that have sliding interfaces.

References

1. Nakano, K., Maegawa, S.: Stick–slip in sliding systems with tangential contact compliance. Tribol. Int. **42**, 1771–1780 (2009)
2. Nakano, K., Maegawa, S.: Occurrence limit of stick–slip: dimensionless analysis for fundamental design of robust–stable systems. Lubr. Sci. **22**, 1–18 (2010)
3. Varenberg, M., Gorb, S.: Shearing of fibrillary adhesive microstructure: friction and shear-related changes in pull-off force. J. R. Soc. Interface **4**, 721–725 (2007)
4. Varenberg, M., Gorb, S.: Hexagonal surface micropattern for dry and wet friction. Adv. Mater. **21**, 483–486 (2009)
5. Murarash, B., Itovich, Y., Varenberg, M.: Tuning elastomer friction by hexagonal surface patterning. Soft Matter **7**, 5553–5557 (2011)
6. Brormann, K., Barel, I., Urbakh, M., Bennewitz, R.: Friction on a microstructured elastomer surface. Tribol. Lett. **50**, 3–15 (2013)
7. Kligerman, Y., Varenberg, M.: Elimination of stick–slip motion in sliding of split or rough surface. Tribol. Lett. **53**, 395–399 (2014)
8. Greiner, C., Schafer, M., Popp, U., Gumbsch, P.: Contact splitting and the effect of dimple depth on static friction of textured surfaces. Adv. Mater. Interface **6**, 7986–7990 (2014)
9. Maegawa, S., Itoigawa, F., Nakamura, T.: Effect of surface grooves on kinetic friction of a rubber slider. Tribol. Int. **102**, 326–332 (2016)
10. Maegawa, S., Itoigawa, F., Nakamura, T.: Effects of stress distribution at the contact interface on static friction force: numerical simulation and model experiment. Tribol. Lett. **62**, 15 (2016)
11. Rubinstein, S.M., Cohen, G., Fineberg, J.: Detachment fronts and the onset of dynamic friction. Nature **430**, 1005–1009 (2004)
12. Rubinstein, S.M., Cohen, G., Fineberg, J.: Dynamics of precursors to frictional sliding. Phys. Rev. Lett. **98**, 226103 (2007)
13. Maegawa, S., Suzuki, A., Nakano, K.: Precursors of global slip in a longitudinal line contact under non-uniform normal loading. Tribol. Lett. **38**, 313–323 (2010)
14. Farkas, Z., Dahmen, S.R., Wolf, D.E.: Static versus dynamic friction: the role of coherence. J. Stat. Mech. Theory Exp. **2005**, P06015 (2005)
15. Hutchings, I.M.: Tribology: Friction and Wear of Engineering Materials. Edward Arnold, London (1992)
16. Maegawa, S., Itoigawa, F., Nakamura, T.: Effect of normal load on friction coefficient for sliding contact between rough rubber surface and rigid smooth plane. Tribol. Int. **92**, 335–343 (2015)
17. Rubinstein, S.M., Cohen, G., Fineberg, J.: Contact area measurements reveal loading-history dependence of static friction. Phys. Rev. Lett. **96**, 256103 (2006)
18. David, O.B., Cohen, G., Fineberg, J.: The dynamics of the onset of frictional slip. Science **330**, 211–214 (2010)
19. Ozaki, S., Inanobe, C., Nakano, K.: Finite element analysis of precursors to macroscopic stick-slip motion in elastic materials: analysis of friction test as a boundary value problem. Tribol. Lett. **55**, 151–163 (2014)
20. Maegawa, S., Itoigawa, F., Nakamura, T.: New insight into the mechanism of static friction: a theoretical prediction of the effect of loading history on static friction base on the static friction model proposed by Lorentz and Persson. Tribol. Int. **102**, 532–539 (2016)